Large-area vertically aligned 2D MoS_2 layers on TEMPO-cellulose nanofibers for biodegradable transient gas sensors

IOP Publishing Nanotechnology
Nanotechnology 33 (2022) 475502 (8pp) https://doi.org/10.1088/1361-6528/ac8811

Large-area vertically aligned 2D MoS_2 layers on TEMPO-cellulose nanofibers for biodegradable transient gas sensors

Changhyeon Yoo[1], Jaesik Yoon[2], Md Golam Kaium[1,3], Brandon Osorto[1], Sang Sub Han[1], Jung Han Kim[4], Bo Kyoung Kim[5], Hee-Suk Chung[5], Dong-Joo Kim[2] and Yeonwoong Jung[1,3,6]

[1] NanoScience Technology Center, University of Central Florida, Orlando, FL 32826, United States of America
[2] Materials Research and Education Center, 275 Wilmore Laboratory, Auburn University, Auburn, AL 36849, United States of America
[3] Department of Materials Science and Engineering, University of Central Florida, Orlando, FL 32816, United States of America
[4] Department of Materials Science and Engineering, Dong-A University, Busan 49315, Republic of Korea
[5] Analytical Research Division, Korea Basic Science Institute, Jeonju 54907, Republic of Korea
[6] Department of Electrical and Computer Engineering, University of Central Florida, Orlando, FL 32816, United States of America

E-mail: yeonwoong.jung@ucf.edu

Received 8 June 2022, revised 26 July 2022
Accepted for publication 9 August 2022
Published 30 August 2022

Abstract

Crystallographically anisotropic two-dimensional (2D) molybdenum disulfide (MoS_2) with vertically aligned (VA) layers is attractive for electrochemical sensing owing to its surface-enriched dangling bonds coupled with extremely large mechanical deformability. In this study, we explored VA-2D MoS_2 layers integrated on cellulose nanofibers (CNFs) for detecting various volatile organic compound gases. Sensor devices employing VA-2D MoS_2/CNFs exhibited excellent sensitivities for the tested gases of ethanol, methanol, ammonia, and acetone; e.g. a high response rate up to 83.39% for 100 ppm ethanol, significantly outperforming previously reported sensors employing horizontally aligned 2D MoS_2 layers. Furthermore, VA-2D MoS_2/CNFs were identified to be completely dissolvable in buffer solutions such as phosphate-buffered saline solution and baking soda buffer solution without releasing toxic chemicals. This unusual combination of high sensitivity and excellent biodegradability inherent to VA-2D MoS_2/CNFs offers unprecedented opportunities for exploring mechanically reconfigurable sensor technologies with bio-compatible transient characteristics.

Supplementary material for this article is available online

Keywords: 2D MoS_2, cellulose nanofiber, flexible device, transient device, gas sensor

(Some figures may appear in colour only in the online journal)

1. Introduction

Transient electronics represents a concept of emerging device technologies with distinctive advantages of improved biological and environmental benignity over conventional approaches [1–3]. In this approach, electronic devices are programmed to be completely disintegrated and transformed into bio-compatible forms upon completing their targeted functions. This transient process is performed in a renewable and recyclable manner, minimally impacting the environment, thus, mitigating the prevalent issue of 'electronic wastes'; i.e. conventional electronic devices are irreversibly disposed and their continued accumulation demands a substantial amount of landfill spaces imposing environmental threats [4–7]. A variety of electronic devices with transient characteristics have been demonstrated for a wide range of applications,

including photovoltaics [8], transistors [9], and medical devices [10, 11]. This idea can be further facilitated by exploring novel inorganic and/or organic materials with essential transient characteristics such as biocompatibility and excellent electrical properties [12–14]. In this regard, recently explored near atom-thickness 2D MoS_2 layers are uniquely promising, owing to their structural, chemical, and electrical superiority. In addition to their property advantages, such as high carrier mobility, they are known to be dissolvable in bio-friendly solutions without releasing any toxic chemicals [15–17]. A combination of these unique yet outstanding characteristics can lead to a variety of novel applications, particularly utilizing their intrinsic capability of detecting various gas species [18–24]. Furthermore, their anisotropic crystallinity allows them to be chemically grown in a vertically aligned (VA) orientation exposing 2D layer edges on their surfaces accompanying mechanical flexibility [18]. These edges-exposed surfaces are chemically reactive due to ample dangling bonds and well suited to electrochemical sensing applications, including the detection of volatile organic compound (VOC) gases [25–28]. Despite the above-projected opportunities, studies on applying transient VA-2D MoS_2 layers for VOC gas sensing remain unavailable.

Herein, we report on VA-2D MoS_2 layers-based VOC gas sensors by employing their high gas sensitivity, excellent mechanical flexibility, and intrinsic transient features. We directly integrated centimeter-scale VA-2D MoS_2 layers onto biodegradable, transparent, and deformable cellulose nanofibers (CNFs) [29–32]. Particularly, 2,2,6,6-tetramethylpiperidine-1-oxyl (TEMPO)-oxidized CNFs, namely TOCNs, were employed owing to their unique advantages such as low density, high stiffness, and large specific surface area [14, 30, 33–35]. VA-2D MoS_2 layers integrated on TOCNs exhibited excellent performance in sensing various VOC gases. For instance, high sensitivity of 83.39% was observed with 100 ppm ethanol, significantly outperforming previously reported sensors based on horizontally aligned 2D MoS_2 layers. Furthermore, the sensors employing VA-2D MoS_2/TOCNs were demonstrated to dissolve in bio-friendly buffer solutions completely. This dissolution was identified to involve the conversion of MoS_2 to non-toxic molybdenum oxide (MoO_x), further confirming the biocompatible transient characteristics of the sensors.

2. Experimental methods

2.1. Chemical vapor deposition (CVD) growth of centimeter-scale VA-2D MoS_2 layers

Mo thin films (6 nm thickness) were deposited on silicon dioxide (300 nm thickness) /silicon (SiO_2/Si) substrates by an e-beam evaporator (Thermionics VE-100) at a deposition rate of ∼0.05–0.12 Å s^{-1} and at a chamber base pressure of $\langle 5.5 \times 10^{-6}$ Torr. The Mo-deposited substrates were placed at the center of a CVD furnace chamber (Lindberg/Blue M Mini-Mite) along with sulfur (S) powder (⩾99.5%, Sigma-Aldrich) placed on an alumina boat on the furnace's upstream side. The CVD chamber was pumped down to 40 mTorr, and ultra-pure Ar gas was supplied at a flow rate of 100 sccm (standard cubic centimeter per minute). Subsequently, the CVD furnace was heated up to 800 °C in ∼50 min and was maintained at that temperature for another ∼50 min, followed by natural cooling down to room temperature.

2.2. Preparation of TOCN substrates and integration of VA-2D MoS_2 layers onto them

Commercially available slurry TOCNs (CELLULOSELAB, width of ∼50 nm and length of > several hundred μm) in water (1 wt%) were mixed with deionized (DI) water followed by sonication for 1–2 h. The prepared well-dispersed TOCN suspension (0.5 wt%) was directly poured onto as-grown VA-2D MoS_2 layers on SiO_2/Si substrates, followed by room-temperature drying for ∼48 h until it turned into a transparent paper. Then, the TOCN-integrated VA-2D MoS_2 layers were manually peeled off from their growth SiO_2/Si substrates.

2.3. Material characterization

Raman spectral characterization was performed with Nanofinder 30 Raman Confocal spectroscopy (Tokyo Instrument Inc.) using a laser source with a wavelength of 532 nm and a spot size of 1 μm. Scanning electron microscope (SEM) characterization was carried out using Hitachi SU8230 at an accelerating voltage of 15 kV with 1 nm resolution. Transmission electron microscope (TEM) characterization was performed with Cs-corrected JEOL ARM 200F at an acceleration voltage of 200 kV. X-ray photoelectron spectroscopy (XPS) characterization was performed with Thermo Scientific ESCALAB 250Xi photoelectron spectrometer using an aluminum (Al) anode as the x-ray source (1486.68 eV). X-ray diffraction (XRD) patterns were measured using Empyrean PANalytical.

2.4. Gas sensing measurement

For the VOS gas sensing measurement, VA-2D MoS_2/TOCN sensors were connected to the resistance measurement equipment (Keithley 2400 source meter) in a closed test chamber (Supplementary information, figure S1 (available online at stacks.iop.org/NANO/33/475502/mmedia)). For the VOC gas injection, the total gas flow was fixed to 40 sccm by combining a mixture of pure nitrogen, pure oxygen, and target gas diluted in nitrogen. The gas carrier is bubbled through the liquid analyte of interest for the gas injection and subsequently mixed with the diluted air in the test chamber. For analyte gas bubbling, the synthetic air comprising 80 sccm of nitrogen and 20 sccm of oxygen gas was continuously blown into the chamber. The resistance of the sensors was recorded by using a customized LabVIEW program under a periodic supply of the target gas.

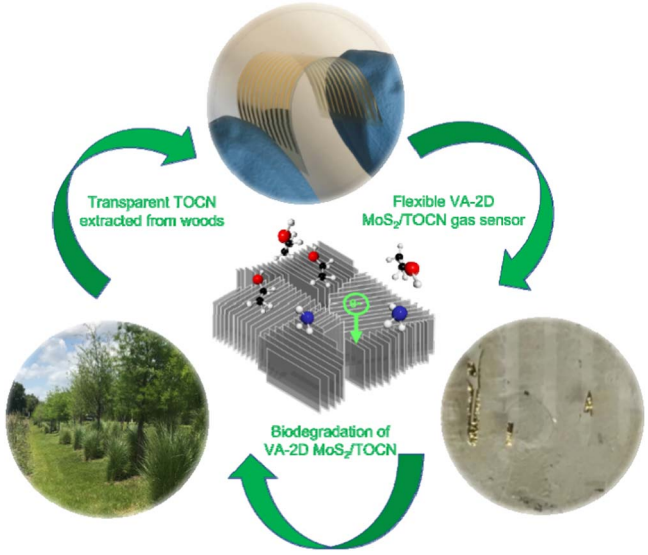

Figure 1. Conceptual illustration of flexible VA-2D MoS_2 layers integrated on TOCN substrates for VOC sensing applications and their biodegradable, transient characteristics.

2.5. Biodegradable dissolution of VA-2D MoS_2/TOCN

Two different buffer solutions (0.1 M) were prepared by dissolving commercially available phosphate-buffered saline (PBS: Sigma Aldrich, pH 7.4, 0.926g) in DI water (100 ml) and dissolving baking soda ($NaHCO_3$, 0.845 g) in DI water (100 ml). VA-2D MoS_2/TOCN sensors with gold (Au) electrodes were placed inside the prepared buffer solutions at 75 °C (hotplate) and were sealed to prevent their rapid evaporation. The samples were taken out of the solutions for ∼20 min for optical microscope observations and the solutions were replaced every 2 d to maintain the same concentration.

3. Results and discussions

Figure 1 presents a conceptual illustration of the likely life cycle of flexible VA-2D MoS_2 layers integrated on TOCN substrates and their biodegradable, transient characteristics. Biodegradable, transparent, and flexible TOCNs are extracted from wood pulps, and they can be naturally biodegraded via fungal biodegradation without causing any deleterious impacts on the environment [14]. VA-2D MoS_2 layers are integrated onto the TOCNs with Au electrode stripes, and they are utilized for VOC gas sensing applications. The gas sensor devices are dissolved via buffer solutions after completing their target functions and are recycled into the environment in an environmentally benign manner. Recently, a variety of *in vivo* and *in vitro* studies indicate the intrinsic biodegradability and biocompatibility of 2D MoS_2 layers; i.e. intrinsically low cytotoxicity was observed in 2D MoS_2 layers when interacting with human cells [36–40], which enabled their application for gene delivery vehicles in biological systems [41–44]. Furthermore, the dissolution of 2D MoS_2 layers in buffer solutions was identified to be bio-friendly [15, 17], which justifies their incorporation into biodegradable TOCNs for the conceptually proposed VOC gas sensors with transient characteristics. The illustration in the center of figure 1 presents a schematic view of VA-2D MoS_2 layers interacting with gas molecules which are adsorbed onto their surface with ample layer edge sites.

Figure 2(a) shows a schematic illustration of the fabrication process of a VA-2D MoS_2/TOCN gas sensor. The fabrication starts with the wafer-scale CVD growth of the VA-2D MoS_2 layers with a typical lateral dimension of ∼10 cm × 2 cm on top of a SiO_2/Si wafer [15, 45–49]. Mo film of a controlled thickness (∼6 nm) is deposited on a clean SiO_2/Si wafer via electron beam evaporation followed by the CVD sulfurization reaction, which converts the Mo films into VA-2D MoS_2 layers, as previously demonstrated [18, 50, 51]. Detailed CVD growth procedures are described in the experimental methods section. Subsequently, TOCN suspension in DI water is drop-casted on the VA-2D MoS_2 layers grown on SiO_2/Si, following the previously developed recipe [15, 45] as described in the experimental methods section. After air-drying at room temperature for ∼48 h, the TOCN-covered VA-2D MoS_2 layers are manually peeled off from the SiO_2/Si wafer [15, 46]. Lastly, Au electrodes in stripe shapes are deposited on top of the VA-2D MoS_2 layers for subsequential electrical measurements. Figure 2(b) shows images of the direct drop-casting of TOCN suspension onto VA-2D MoS_2 layers grown on a SiO_2/Si sample (left) and a manually peeled VA-2D MoS_2/TOCN sample and its original SiO_2/Si wafer (right). Figure 2(c) presents images of a completely fabricated VA-2D MoS_2/TOCN gas sensor in its pristine (left) and bent (right) state, confirming its mechanical flexibility. Figure 2(d) shows the Raman spectroscopy profile obtained from the sample in figure 2(c), revealing the characteristic peaks of VA-2D MoS_2 layers corresponding to the in-plane (E_{2g}^1, at 381 cm^{-1}) and out-of-plane (A_{1g}, at 407 cm^{-1}) vibration modes. The low peak intensity ratio, i.e. E_{2g}^1/A_{1g} of ∼0.5, indicates the dominance of the A_{1g} vibration mode owing to the pronouncedly exposed layer edge sites on the sample surface, consistent with previous studies [47, 48, 52]. Figure 2(e) shows SEM images of an as-prepared TOCN film before (top) and after (bottom) the integration of VA-2D MoS_2 layers, confirming its continuous film morphology. The corresponding higher magnification SEM images are presented in Supplementary Information, figure S2. Figure 2(f) shows energy-dispersive x-ray spectroscopy (EDS) mapping images of Mo and S elements obtained from the sample in figure 2(b), confirming their spatial homogeneity. Figure 2(g) shows a plain-view high-resolution transmission electron microscopy (HRTEM) image of as-grown VA-2D MoS_2 layers unveiling their surface-exposed 2D layer edges sites, consistent with previous studies [18, 47, 50, 52–54]. The measured lattice spacing of ∼0.62 nm confirms the presence of highly-dense surface-exposed van der Waals (vdW) gaps. The corresponding fast Fourier-transform image shows a (002) diffraction ring, further indicating predominantly surface-exposed vdW gaps, as presented in Supplementary information, figure S3. Additionally, an XRD pattern obtained from VA-2D MoS_2 layers

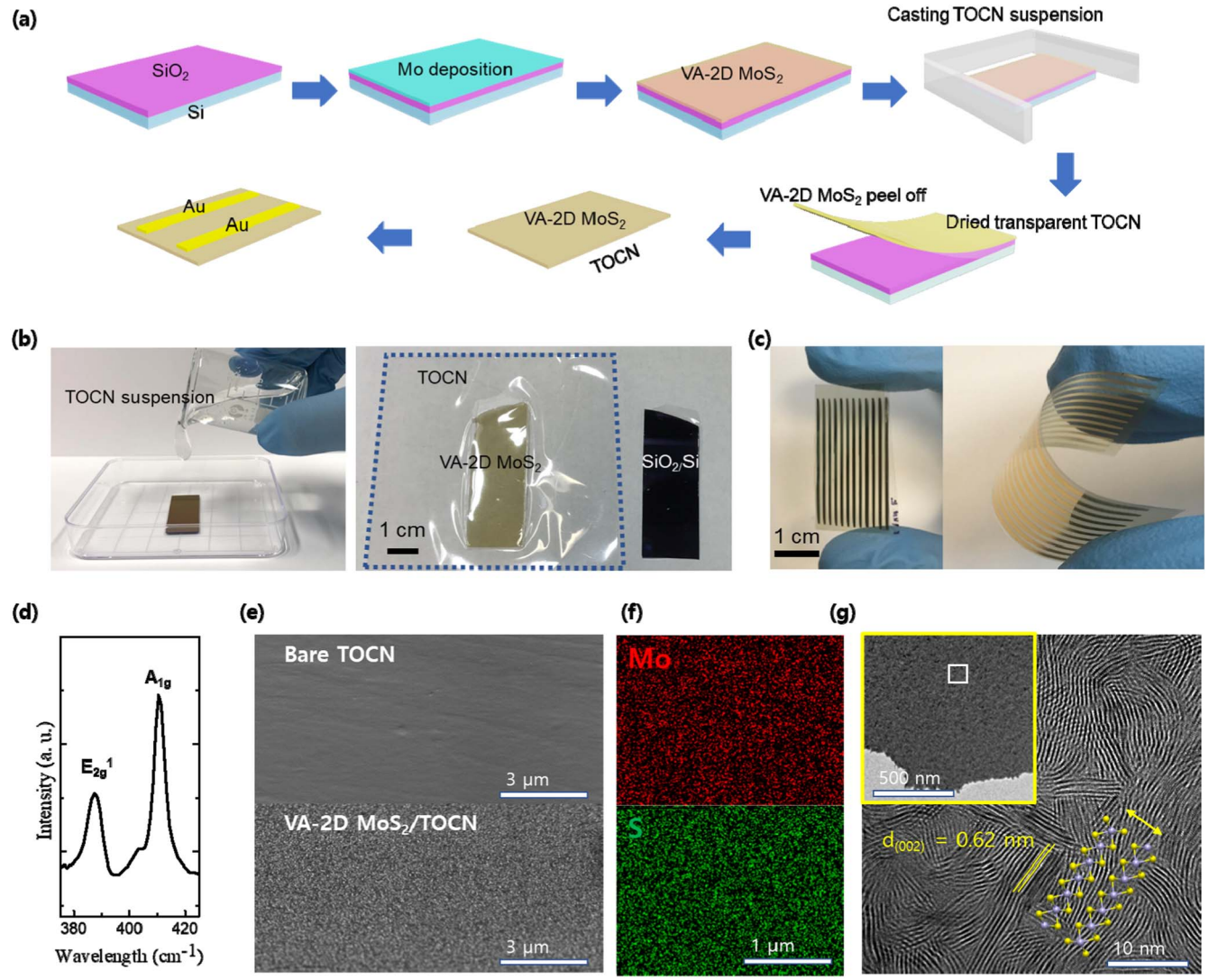

Figure 2. Material preparation and characterization of VA-2D MoS_2 layers integrated on TOCN substrates. (a) Schematic illustration of the fabrication process of VA-2D MoS_2/TOCN gas sensor. (b) Camera images of TOCN suspension drop-casting on VA-2D MoS_2 layers grown on a SiO_2/Si substrate (left) and integrated VA-2D MoS_2 layers on dried TOCN (right). (c) Optical images of VA-2D MoS_2/TOCN sensor with Au electrodes in its pristine (left) and bent (right) state. (d) Raman spectrum of the sample in (c) showing characteristic peaks of VA-2D MoS_2 layers. (e) SEM images of a bare TOCN (top) and VA-2D MoS_2 integrated on it (bottom). (f) SEM-EDS elemental maps showing the spatial distribution of Mo and S in VA-2D MoS_2 layers. (g) Plain-view HRTEM image of VA-2D MoS_2 layers revealing layer edge sites and its corresponding low magnification image (inset).

grown on a SiO_2/Si wafer before their integration on TOCN is presented in Supplementary Information, figure S4.

Figures 3(a)–(d) present the dynamic gas-sensing performances of a VA-2D MoS_2/TOCN sensor tested with four different VOC gases of methanol, ethanol, acetone, and ammonia. The VA-2D MoS_2/TOCN sensor was periodically exposed to the gases of constant 100 ppm for 5 min under an ambient atmosphere at room temperature, and its base resistance was ~40 kΩ. After the introduction of each gas, the sensor was exposed to a flow of clean air composed of nitrogen (80 sccm) and oxygen (20 sccm) to recover its base resistance. During the introduction of all tested gases, the sensor exhibited an increase in its resistance which returned to the base value within 5 min upon their termination. The sensor reliably responded to the three repeated ON/OFF gas cycles, confirming its excellent sensitivity and reproducibility. Response/recovery times are commonly adopted to identify the proficiency of sensors, which are defined by the timelines where they reach 90% of total resistance changes [20, 55]. The average response/recovery times are determined to be in a range of ~100 to ~300s for our tested VOC gases, as presented in Supplementary information, figure S5. CVD-grown VA-2D MoS2 layers are known to exhibit p-type semiconducting characteristics, as verified in previous studies [18, 56, 57]. Given all the tested gases are known to be electron donor molecules [58, 59], they tend to transfer electrons to the VA-2D MoS_2 layers upon being adsorbed onto the surface-exposed layer edge sites. Accordingly, the concentration of charge carriers (i.e. hole concentration) on the surface of the VA-2D MoS_2 layers decreases, leading to the increased resistance of the sensor. This resistance increase introduced by the electron-donating VOC gases is opposite to

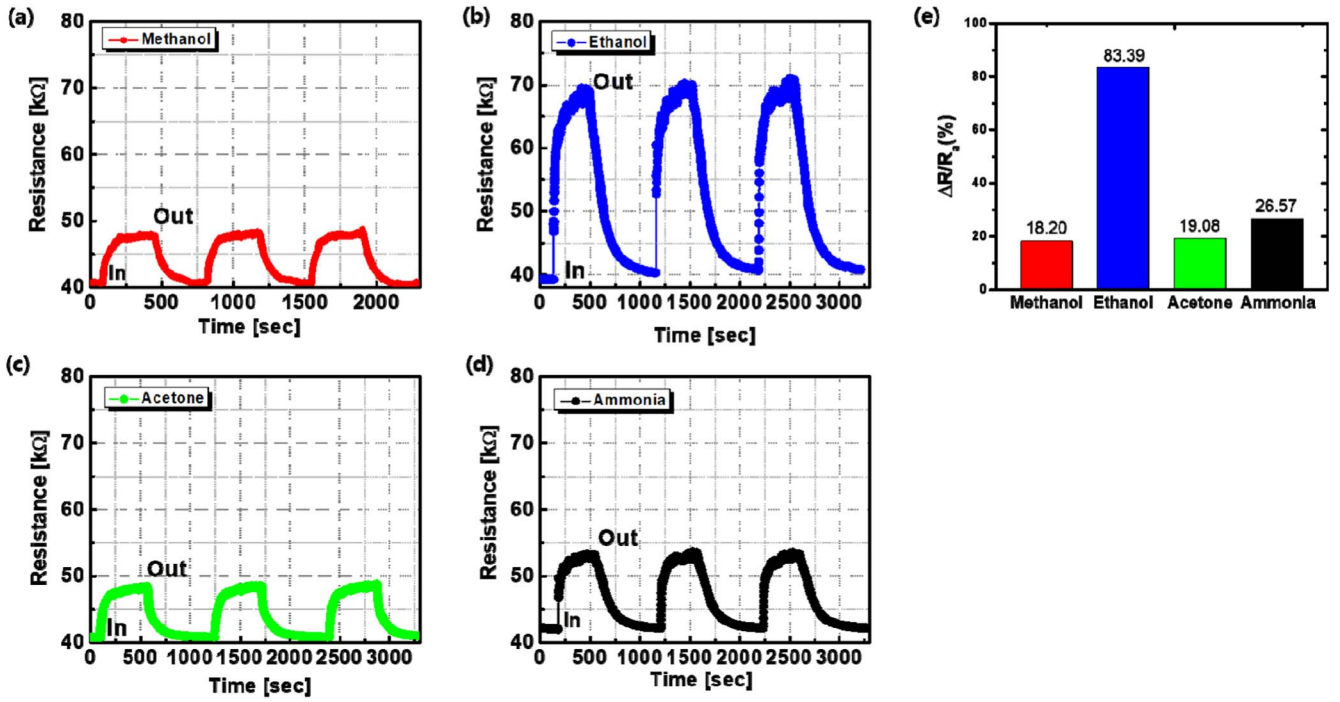

Figure 3. VOC gas sensing demonstrations with VA-2D MoS_2/TOCNs under a cyclic introduction of 100 ppm (a) methanol, (b) ethanol, (c) acetone, and (d) ammonia. (e) Calculated average gas response for each gas.

the observation with the electron-accepting nitrogen dioxide (NO_2) gas, which indeed decreased the resistance of VA-2D MoS_2 layers, as previously reported [18]. Figure 3(e) compares the calculated average gas response for each gas presented by the relative ratio of resistance, i.e. $\Delta R/R_a = (R_{\text{gas on}} - R_a)/R_a$ where ΔR is the resistance change caused by the gas, $R_{\text{gas on}}$ is the resistance when the gas was introduced, and R_a is the base resistance under the ambient air. The gas response was identified to be 18.20%, 83.39%, 19.08%, and 26.57% for methanol, ethanol, acetone, and ammonia, respectively. It is noteworthy that this VA-2D MoS_2 layers-based sensor exhibited the highest gas response of 83.39% with ethanol gas. This responsitivity value is indeed much higher than those observed with horizontally-aligned 2D MoS_2 layers-based sensors employed for sensing 100 ppm ethanol gas in previous studies [19, 23, 24], confirming the structural advantage of VA-2D MoS_2 layers. While the exact clarification of the origin for this superior ethanol sensitivity in VA-2D MoS_2 layers needs further investigation, several possible mechanisms are proposed. For instance, the presence of high-density $(–CH_2–)_n$ chains within ethanol is suggested to be responsible for its facile surface decomposition, resulting in a more efficient transfer of electrons than methanol [60]. This was verified by density functional theory (DFT) studies which confirmed the negative adsorption energy of ethanol and various VOC gases, including methanol, suggesting its easier electrochemical detection [20]. This strong binding affinity of ethanol was further facilitated by the high *d*-orbital electron density of 2D MoS_2 layer edge sites inherent to VA-2D MoS_2 layers, as previously demonstrated in additional DFT studies [53].

Having confirmed the excellent sensitivity of VA-2D MoS_2/TOCN gas sensors, we focused on unveiling their biodegradable transient characteristics. As 2D MoS_2 layers are known to be water-insoluble [61] and highly stable under ambient conditions [62–65], we attempted to dissolve VA-2D MoS_2 layers in two different bio-friendly buffer solutions of PBS and BSB [15–17]. Details for the preparation of these buffer solutions and the dissolution experiments are presented in the experimental methods section. Figure 4(a) shows time-lapse images of VA-2D MoS_2/TOCN with Au electrodes undergoing dissolution in PBS solution (100 ml of 0.1 M) set at 75 °C with pH ~6.7. The top camera images reveal that VA-2D MoS_2 layers gradually disintegrate with increasing time and become completely dissolved after ~6 d, and the bottom optical microscope images present the corresponding enlarged views of their progressive disintegration. Figure 4(b) shows a camera image of the PBS solution containing the dissolved VA-2D MoS_2 layers after 6 d, revealing some fragmented Au electrode residuals. Figure 4(c) shows time-lapse images of VA-2D MoS_2/TOCN with Au electrodes undergoing dissolution in the BSB solution composed of sodium bicarbonate ($NaHCO_3$) mixed with DI water (100 ml of 0.1 M) at 75 °C with pH ~8.3. The images reveal the transient characteristics of VA-2D MoS_2/TOCN, similar to the observation with PBS solution in figure 4(a). Figure 4(d) shows a camera image of the BSB solution containing the dissolved VA-2D MoS_2 layers after 6 d, revealing similar characteristics observed with PBS solution (figure 4(b)). In both figures 4(a) and (c), it is noted that the cracks formed on the surfaces of VA-2D MoS_2 layers after ~24 h of exposure to buffer solutions serve as the reaction starting points spreading towards outer regions, which is an indication of

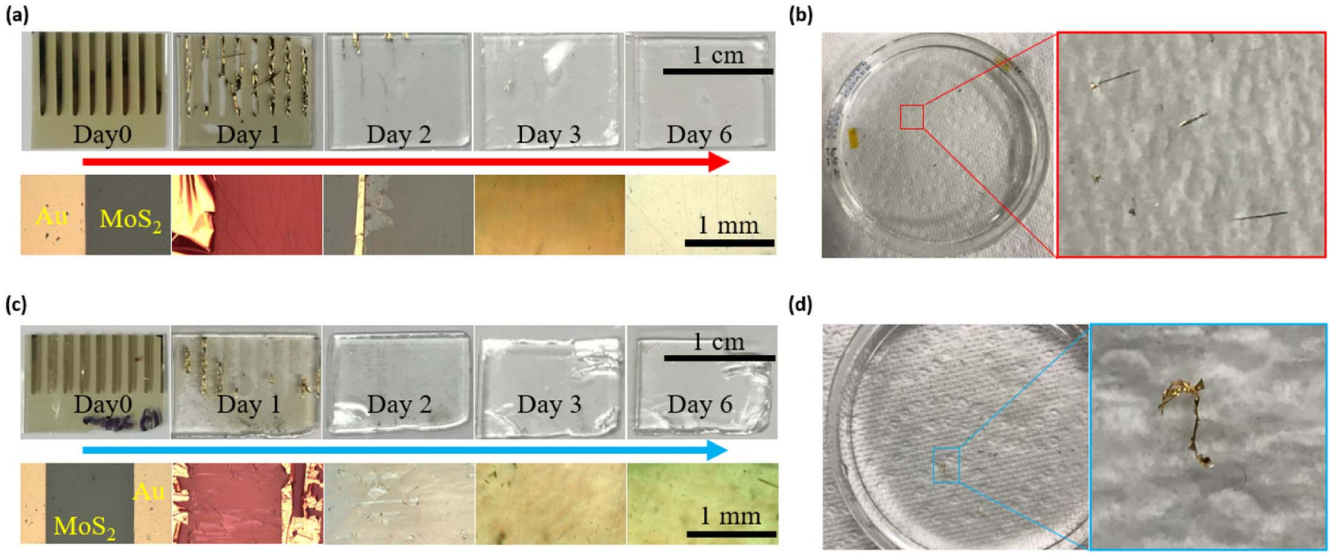

Figure 4. Demonstration of biodegradable transient characteristics. (a) Dissolution of VA-2D MoS_2/TOCN with Au electrodes in PBS solution at 75 °C. (b) Residual Au electrodes in PBS solution after 6 d. (c) Dissolution of VA-2D MoS_2/TOCN with Au electrodes in BSB solution at 75 °C. (d) Residual Au electrodes in BSB solution after 6 d.

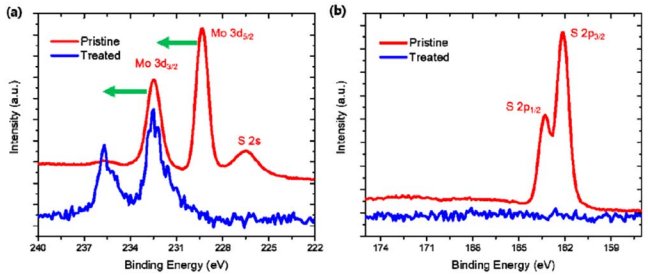

Figure 5. XPS spectra obtained from VA-2D MoS_2 layers before (red lots) and after (blue plots) their dissolution in BSB solution, denoting peak shifts of (a) Mo 3d and S 2s (b) S 2p core levels.

defect-accelerated degradation [12, 17]. Potassium/sodium ions (K^+/ Na^+) contained in PBS and Na^+ in BSB solutions are known to distort the lattice of 2D MoS_2 layers via intercalation into their vdW gaps, and subsequently form soluble potassium/sodium sulfides (K_2S/Na_2S) and molybdenum di/trioxides (MoO_2/MoO_3) [12, 15, 17, 66].

In order to clarify the dissolution chemistry and mechanism of VA-2D MoS_2 layers in buffer solutions, we employed x-ray photoelectron spectroscopy (XPS) to characterize their oxidation states. Figure 5 shows XPS spectra obtained from VA-2D MoS_2 layers before and after their exposure to BSB solution. Figure 5(a) compares XPS peaks corresponding to Mo 3d and S 2s core levels obtained from an identical sample in its pristine state (red plot) and after being treated with BSB solution for 8 d (blue plot). The sample in its pristine state exhibits peaks at 232.5, 229.3, and 226.5 eV, which correspond to Mo $3d_{3/2}$, Mo $3d_{5/2}$, and S 2s, respectively. Meanwhile, it exhibits a noticeable shift of Mo peaks, i.e. located at 235.7 and 232.5 eV, which indicates a stoichiometric change of Mo (IV) to Mo (V) oxidation state, similar to previous observations [15]. Figure 5(b) compares XPS peaks corresponding to S 2p core levels obtained from the same sample before/after its BSB treatment. The pristine sample exhibits two characteristic peaks at 163.3 and 162.1 eV corresponding to S $2p_{1/2}$ and S $2p_{3/2}$, respectively, indicating a presence of stoichiometric sulfide (S^{2-}) in VA-2D MoS_2 layers. These sulfide peaks completely disappear after the treatment, which, together with the XPS spectra of figure 5(a), confirms the conversion of stoichiometric MoS_2 to bio-friendly MoO_x. In addition to confirming the dissolution of VA-2D MoS_2 layers, it is worth mentioning that noble metals such as Au are also dissolvable in various buffer solutions, which can release chloride ions in a bio-friendly manner [67]. For XPS measurements, all spectra were referenced to an Au ($4f_{7/2}$) binding energy of 84.0 eV and compared with previous studies from the National Institute of Standards and Technology photoelectron database [68–72].

4. Conclusion

In summary, we developed mechanically flexible VA-2D MoS_2/TOCN gas sensors and demonstrated their VOC gas sensing performances at room temperature. The gas sensors successfully detected four different tested gases of 100 ppm, including ethanol, methanol, acetone, and ammonia. They exhibited extremely high sensitivity, particularly for ethanol gas, surpassing previously explored 2D MoS_2-based sensors employing horizontally-aligned 2D layers. Furthermore, their intrinsic biodegradable and transient characteristics were demonstrated with various bio-friendly buffer solutions. This study broadens the versatility and applicability of VA-2D MoS_2 layers for futuristic unconventional device applications.

Acknowledgments

This research was supported by the US National Science Foundation (CAREER: 2142310).

Data availability statement

All data that support the findings of this study are included within the article (and any supplementary files).

ORCID iDs

Changhyeon Yoo https://orcid.org/0000-0003-0649-0445
Brandon Osorto https://orcid.org/0000-0003-1227-823X
Yeonwoong Jung https://orcid.org/0000-0001-6042-5551

References

[1] Fu K K, Wang Z, Dai J, Carter M and Hu L 2016 Transient electronics: materials and devices *Chem. Mater.* **28** 3527–39
[2] Li R, Wang L, Kong D and Yin L 2018 Recent progress on biodegradable materials and transient electronics *Bioact. Mater.* **3** 322–33
[3] Jamshidi R, Taghavimehr M, Chen Y, Hashemi N and Montazami R 2022 Transient electronics as sustainable systems: from fundamentals to applications *Adv. Sustain. Syst.* **6** 2100057
[4] Robinson B H 2009 E-waste: an assessment of global production and environmental impacts *Sci. Total Environ.* **408** 183–91
[5] Perkins D N, Brune Drisse M-N, Nxele T and Sly P D 2014 E-waste: a global hazard *Ann. Glob. Health* **80** 286–95
[6] Hossain M S, Al-Hamadani S M Z F and Rahman M T 2015 E-waste: a challenge for sustainable development *J. Health Pollut.* **5** 3–11
[7] Ahirwar R and Tripathi A K 2021 E-waste management: a review of recycling process, environmental and occupational health hazards, and potential solutions *Environ. Nanotechnol. Monit. Manag.* **15** 100409
[8] Hwang S-W *et al* 2012 A physically transient form of silicon electronics *Science* **337** 1640–4
[9] Bettinger C J and Bao Z 2010 Organic Thin-film transistors fabricated on resorbable biomaterial substrates *Adv. Mater.* **22** 651–5
[10] Irimia-Vladu M *et al* 2010 Biocompatible and biodegradable materials for organic field-effect transistors *Adv. Funct. Mater.* **20** 4069–76
[11] Tao H *et al* 2014 Silk-based resorbable electronic devices for remotely controlled therapy and *in vivo* infection abatement *Proc. Natl Acad. Sci. USA* **111** 17385–9
[12] Chen X, Shinde S, Dhakal K, Lee S, Kim H, Lee Z and Ahn J-H 2018 Degradation behaviors and mechanisms of MoS_2 crystals relevant to bioabsorbable electronics *NPG Asia Mater.* **10** 810–20
[13] Hosseini E S, Dervin S, Ganguly P and Dahiya R 2021 Biodegradable materials for sustainable health monitoring devices *ACS Appl. Bio Mater.* **4** 163–94
[14] Jung Y H *et al* 2015 High-performance green flexible electronics based on biodegradable cellulose nanofibril paper *Nat. Commun.* **6** 7170
[15] Yoo C *et al* 2020 Wafer-scale two-dimensional MoS_2 layers integrated on cellulose substrates toward environmentally friendly transient electronic devices *ACS Appl. Mater. Interfaces* **12** 25200–10
[16] Aracena A, Rubilar R, Jerez O and Carvajal D 2015 Dissolution of MoS_2 concentrate using NaClO from 283 to 373 K *Can. Metall. Q.* **54** 455–9
[17] Chen X *et al* 2018 CVD-grown monolayer MoS_2 in bioabsorbable electronics and biosensors *Nat. Commun.* **9** 1690
[18] Islam M A *et al* 2020 Vertically aligned 2D MoS_2 layers with strain-engineered serpentine patterns for high-performance stretchable gas sensors: experimental and theoretical demonstration *ACS Appl. Mater. Interfaces* **12** 53174–83
[19] Singh S, Raj S and Sharma S 2021 Ethanol sensing using MoS_2/TiO_2 composite prepared via hydrothermal method *Mater. Today Proc.* **46** 6083–6
[20] Yap S H K, Chan K K, Yeh C-H, Chien Y-H and Yong K-T 2021 Two-dimensional MoS_2 nanosheet-functionalized optical microfiber for room-temperature volatile organic compound detection *ACS Appl. Nano Mater.* **4** 13440–9
[21] Zhang J, Li T, Guo J, Hu Y and Zhang D 2021 Two-step hydrothermal fabrication of CeO_2-loaded MoS_2 nanoflowers for ethanol gas sensing application *Appl. Surf. Sci.* **568** 150942
[22] Burman D, Raha H, Manna B, Pramanik P and Guha P K 2021 Substitutional doping of MoS_2 for superior gas-sensing applications: a proof of concept *ACS Sens.* **6** 3398–408
[23] Singh S and Sharma S 2022 Temperature-based selective detection of hydrogen sulfide and ethanol with MoS_2/WO_3 composite *ACS Omega* **7** 6075–85
[24] Liu L, Yang W, Zhang H, Yan X and Liu Y 2022 Ultra-high response detection of alcohols based on CdS/MoS_2 composite *Nanoscale Res. Lett.* **17** 7
[25] Yang S, Jiang C and Wei S-H 2017 Gas sensing in 2D materials *Appl. Phys. Rev.* **4** 021304
[26] Ko K Y *et al* 2016 Improvement of gas-sensing performance of large-area tungsten disulfide nanosheets by surface functionalization *ACS Nano* **10** 9287–96
[27] Liu X, Ma T, Pinna N and Zhang J 2017 Two-dimensional nanostructured materials for gas sensing *Adv. Funct. Mater.* **27** 1702168
[28] Kim T H, Kim Y H, Park S Y, Kim S Y and Jang H W 2017 Two-dimensional transition metal disulfides for chemoresistive gas sensing: perspective and challenges *Chemosensors* **5** 15
[29] Moon R J, Martini A, Nairn J, Simonsen J and Youngblood J 2011 Cellulose nanomaterials review: structure, properties and nanocomposites *Chem. Soc. Rev.* **40** 3941–94
[30] Eichhorn S J 2011 Cellulose nanowhiskers: promising materials for advanced applications *Soft Matter* **7** 303–15
[31] Kim J-H, Shim B S, Kim H S, Lee Y-J, Min S-K, Jang D, Abas Z and Kim J 2015 Review of nanocellulose for sustainable future materials *Int. J. Precis. Eng. Manuf. - Green Technol.* **2** 197–213
[32] Kang W, Yan C, Foo C Y and Lee P S 2015 Foldable electrochromics enabled by nanopaper transfer method *Adv. Funct. Mater.* **25** 4203–10
[33] Saito T, Kimura S, Nishiyama Y and Isogai A 2007 Cellulose nanofibers prepared by TEMPO-mediated oxidation of native cellulose *Biomacromolecules* **8** 2485–91
[34] Isogai A, Saito T and Fukuzumi H 2011 TEMPO-oxidized cellulose nanofibers *Nanoscale* **3** 71–85
[35] Yang W, Jiao L, Liu W and Dai H 2019 Manufacture of highly transparent and hazy cellulose nanofibril films via coating TEMPO-oxidized wood fibers *Nanomaterials* **9** 107
[36] Fan J, Li Y, Nguyen H N, Yao Y and Rodrigues D F 2015 Toxicity of exfoliated-MoS_2 and annealed exfoliated-MoS_2 towards planktonic cells, biofilms, and mammalian cells in the presence of electron donor *Environ. Sci. Nano* **2** 370–9
[37] Liu T, Wang C, Gu X, Gong H, Cheng L, Shi X, Feng L, Sun B and Liu Z 2014 Drug delivery with pegylated MoS_2 nano-sheets for combined photothermal and chemotherapy of cancer *Adv. Mater.* **26** 3433–40
[38] Wang X *et al* 2015 Differences in the toxicological potential of 2D versus aggregated molybdenum disulfide in the lung *Small* **11** 5079–87

[39] Yadav V, Roy S, Singh P, Khan Z and Jaiswal A 2019 2D MoS_2-based nanomaterials for therapeutic, bioimaging, and biosensing applications *Small* **15** 1803706

[40] Li B L, Setyawati M I, Chen L, Xie J, Ariga K, Lim C-T, Garaj S and Leong D T 2017 Directing assembly and disassembly of 2D MoS_2 nanosheets with DNA for drug delivery *ACS Appl. Mater. Interfaces* **9** 15286–96

[41] Wang L, Wang Y, Wong J I, Palacios T, Kong J and Yang H Y 2014 Functionalized MoS_2 nanosheet-based field-effect biosensor for label-free sensitive detection of cancer marker proteins in solution *Small* **10** 1101–5

[42] Chen S-C, Lin C-Y, Cheng T-L and Tseng W-L 2017 6-Mercaptopurine-induced fluorescence quenching of monolayer MoS_2 nanodots: applications to glutathione sensing, cellular imaging, and glutathione-stimulated drug delivery *Adv. Funct. Mater.* **27** 1702452

[43] Gu W, Yan Y, Cao X, Zhang C, Ding C and Xian Y 2016 A facile and one-step ethanol-thermal synthesis of MoS_2 quantum dots for two-photon fluorescence imaging *J. Mater. Chem. B* **4** 27–31

[44] Kou Z *et al* 2014 A promising gene delivery system developed from PEGylated MoS_2 nanosheets for gene therapy *Nanoscale Res. Lett.* **9** 587

[45] Yoo C, Ko T-J, Han S S, Shawkat M S, Oh K H, Kim B K, Chung H-S and Jung Y 2021 Mechanically rollable photodetectors enabled by centimetre-scale 2D MoS_2 layer/TOCN composites *Nanoscale Adv.* **3** 3028–34

[46] Kim J H, Ko T-J, Okogbue E, Han S S, Shawkat M S, Kaium M G, Oh K H, Chung H-S and Jung Y 2019 Centimeter-scale green integration of layer-by-layer 2D TMD vdW heterostructures on arbitrary substrates by water-assisted layer transfer *Sci. Rep.* **9** 1641

[47] Choudhary N, Chung H S, Kim J H, Noh C, Islam M A, Oh K H, Coffey K, Jung Y and Jung Y 2018 Strain-driven and layer-number-dependent crossover of growth mode in van der Waals heterostructures: 2D/2D layer-by-layer horizontal epitaxy to 2D/3D vertical reorientation *Adv. Mater. Interfaces* **5** 1800382

[48] Kong D, Wang H, Cha J J, Pasta M, Koski K J, Yao J and Cui Y 2013 Synthesis of MoS_2 and $MoSe_2$ films with vertically aligned layers *Nano Lett.* **13** 1341–7

[49] Jung Y, Shen J, Liu Y, Woods J M, Sun Y and Cha J J 2014 Metal seed layer thickness-induced transition from vertical to horizontal growth of MoS_2 and WS_2 *Nano Lett.* **14** 6842–9

[50] Hwang J-H, Islam M A, Choi H, Ko T-J, Rodriguez K L, Chung H-S, Jung Y and Lee W H 2019 Improving electrochemical Pb^{2+} detection using a vertically aligned 2D MoS_2 nanofilm *Anal. Chem.* **91** 11770–7

[51] Han S S *et al* 2019 Horizontal-to-vertical transition of 2D layer orientation in low-temperature chemical vapor deposition-grown $PtSe_2$ and its influences on electrical properties and device applications *ACS Appl. Mater. Interfaces* **11** 13598–607

[52] Islam M A, Church J, Han C, Chung H-S, Ji E, Kim J H, Choudhary N, Lee G-H, Lee W H and Jung Y 2017 Noble metal-coated MoS_2 nanofilms with vertically-aligned 2D layers for visible light-driven photocatalytic degradation of emerging water contaminants *Sci. Rep.* **7** 14944

[53] Cho S-Y, Kim S J, Lee Y, Kim J-S, Jung W-B, Yoo H-W, Kim J and Jung H-T 2015 Highly enhanced gas adsorption properties in vertically aligned MoS_2 layers *ACS Nano* **9** 9314–21

[54] Wang M *et al* 2019 Structural evolutions of vertically aligned two-dimensional MoS_2 layers revealed by *in situ* heating transmission electron microscopy *J. Phys. Chem. C* **123** 27843–53

[55] Lee E, Yoon Y S and Kim D-J 2018 Two-dimensional transition metal dichalcogenides and metal oxide hybrids for gas sensing *ACS Sens.* **3** 2045–60

[56] Park J, Choudhary N, Smith J, Lee G, Kim M and Choi W 2015 Thickness modulated MoS_2 grown by chemical vapor deposition for transparent and flexible electronic devices *Appl. Phys. Lett.* **106** 012104

[57] McDonnell S, Addou R, Buie C, Wallace R M and Hinkle C L 2014 Defect-dominated doping and contact resistance in MoS_2 *ACS Nano* **8** 2880–8

[58] Miller D R, Akbar S A and Morris P A 2014 Nanoscale metal oxide-based heterojunctions for gas sensing: a review *Sensors Actuators B* **204** 250–72

[59] Lee E, VahidMohammadi A, Prorok B C, Yoon Y S, Beidaghi M and Kim D-J 2017 Room temperature gas sensing of two-dimensional titanium carbide (MXene) *ACS Appl. Mater. Interfaces* **9** 37184–90

[60] Giberti A, Casotti D, Cruciani G, Fabbri B, Gaiardo A, Guidi V, Malagù C, Zonta G and Gherardi S 2015 Electrical conductivity of CdS films for gas sensing: Selectivity properties to alcoholic chains *Sensors Actuators B* **207** 504–10

[61] Haynes W M 2014 *CRC Handbook of Chemistry and Physics* (Boca Raton, FL: CRC Press)

[62] Kc S, Longo R C, Wallace R M and Cho K 2015 Surface oxidation energetics and kinetics on MoS_2 monolayer *J. Appl. Phys.* **117** 135301

[63] Mirabelli G *et al* 2016 Air sensitivity of MoS_2, $MoSe_2$, $MoTe_2$, HfS_2, and $HfSe_2$ *J. Appl. Phys.* **120** 125102

[64] Longo R C, Addou R, Santosh K, Noh J-Y, Smyth C M, Barrera D, Zhang C, Hsu J W, Wallace R M and Cho K 2017 Intrinsic air stability mechanisms of two-dimensional transition metal dichalcogenide surfaces: basal versus edge oxidation *2D Mater.* **4** 025050

[65] Rao R, Islam A E, Campbell P M, Vogel E M and Maruyama B 2017 *In situ* thermal oxidation kinetics in few layer MoS_2 *2D Mater.* **4** 025058

[66] Wang X, Shen X, Wang Z, Yu R and Chen L 2014 Atomic-scale clarification of structural transition of MoS_2 upon sodium intercalation *ACS Nano* **8** 11394–400

[67] Cherevko S, Topalov A A, Zeradjanin A R, Katsounaros I and Mayrhofer K J J 2013 Gold dissolution: towards understanding of noble metal corrosion *RSC Adv.* **3** 16516–27

[68] Naumkin A, Kraut-Vass A, Gaarenstroom S and Powell C 2012 NIST X-ray photoelectron spectroscopy (XPS) database, version 4.1 can be found under (http://srdata.nist.gov/xps) (https://doi.org/10.18434/T4T88K)

[69] Choi J G and Thompson L T 1996 XPS study of as-prepared and reduced molybdenum oxides *Appl. Surf. Sci.* **93** 143–9

[70] Martín-Luengo A T, Köstenbauer H, Winkler J and Bonanni A 2017 Processing and charge state engineering of MoO_x *AIP Adv.* **7** 015034

[71] Moulder J F, Stickle W F, Sobol P E and Bomben K D 1992 *Handbook of X-ray Photoelectron Spectroscopy* (United States: Physical Electronics Division, Perkin-Elmer Corporation)

[72] Hofmann S 2012 *Auger-and X-ray Photoelectron Spectroscopy in Materials Science: A User-Oriented Guide* vol 49 (New York: Springer)